Aerosol-assisted Chemical Vapor Deposition of V_2O_5 Cathodes with High Rate Capabilities for Magnesium-ion Batteries

Charalampos Drosos,[1] Chenglin Jia,[2] Shiny Mathew,[2] Robert G. Palgrave,[2] Benjamin Moss,[3] Andreas Kafizas,[3] and Dimitra Vernardou[4]**

[1]Delta Nano – Engineering Solutions Ltd., England, UK, www.delta-nano.com, info@delta-nano.com
[2]Department of Chemistry, University College London, 20 Gordon Street, London, WC1H 0AJ, UK
[3]Department of Chemistry, Imperial College London, South Kensington Campus, London, SW7 2AZ, UK
[4]Center of Materials Technology and Photonics, School of Applied Technology, Technological Educational Institute of Crete, 710 04 Heraklion, Crete, Greece

Corresponding authors: a.kafizas@imperial.ac.uk, dimitra@iesl.forth.gr

Abstract

The growth of orthorhombic vanadium pentoxide nanostructures was accomplished using an aerosol-assisted chemical vapor deposition process. These materials showed excellent electrochemical performance for magnesium-ion storage in an aqueous electrolyte; showing specific discharge capacities of up to 427 mAh g^{-1} with a capacity retention of 82 % after 2000 scans under a high specific current of 5.9 A g^{-1}. The high rate capability suggested good structural stability and high reversibility. We believe the development of low-cost and large-area coating methods, such as the technique used herein, will be essential for the upscalable fabrication of next-generation rechargeable battery technologies.

Keywords: Mg-ion battery, V_2O_5, cathode, aqueous electrolyte, aerosol-assisted chemical vapor deposition (AACVD)

1. Introduction

The development of energy storage technology is undoubtedly one of the greatest challenges faced by modern society today [1,2]. Our over-dependence on fossil fuels has

resulted in global warming and high levels of pollution in cities primarily due to emissions from vehicles. As such, battery powered cars are being developed to reduce pollution in cities. Rechargeable Li-ion batteries are widely utilized in mobile electronic devices and electric cars due to their high energy density, cycle stability and energy efficiency [3-5]. Although, they have been optimized to meet the requirements for portable electronics, the increasing demands for automotive needs require greater energy density, high safety, low cost and longer stability [6].

Magnesium-ion batteries (MIBs) are a promising alternative [7], due to the high abundance of magnesium (1.94 %) compared with lithium resources (0.006 %) [8,9]. MIBs based on aqueous electrolytes are a good option for large scale applications since the water-based battery system is safer than combustible organic electrolytes. Additionally, aqueous electrolyte solutions are cheap and the assembly process of batteries is effortless since the need for an inert atmosphere in the production line is eliminated. As such, the potential improvements in capacity and stability in water-based Mg-ion battery systems has aroused widespread attention due to: a) the absence of solid electrolyte interface at the electrode/electrolyte boundary in aqueous solutions, b) two-electron storage per Mg-ion and c) the analogous ionic radius of Mg^{2+} (r ~ 0.89 Å) as compared with Li^{+} (r ~ 0.92 Å) (NOTE: aqueous sodium-ion batteries typically display poor stability resulting from the larger radius of Na^{+} ions, r ~ 1.18 Å) [10].

Vanadium pentoxide (V_2O_5) is one of the most promising cathode materials for MIBs due to its low cost, high earth abundant resources and theoretical capacity (440 mAh g^{-1}) [11]. Apart from efficient Li^{+} intercalation/de-intercalation [12], V_2O_5 also shows promising Mg^{2+} intercalation/de-intercalation performance [13]. Nevertheless, the majority of examinations thus far has been based on organic electrolytes [14], and scarcely focused on aqueous electrolytes.

In this work, aerosol-assisted chemical vapor deposition (AACVD) was used to grow V_2O_5 cathodes. AACVD was chosen to grow our cathodes because it is a synthetic method that is compatible with in-line manufacturing processes, where material properties such as material thickness, phase and nanostructure can be precisely controlled by simply varying parameters such as the growth temperature, precursor composition and flow rate. Using this method, one can grow strongly adhered V_2O_5 coatings of well-defined size, shape and crystallinity that show promising performance for Mg-ion storage. As such, we believe the development of low-cost and large-area coating methods, such as AACVD, may play a significant role in the upscalable fabrication of next-generation rechargeable battery technologies.

2. Experimental

Synthesis of V_2O_5 cathodes: Thin films of V_2O_5 were grown on fluorine-doped tin oxide (FTO) glass electrodes using AACVD. The vanadium precursor, vanadium (V) oxytri-isopropoxide (0.24 g, 1 mmol) was dissolved in 2-methoxy-ethanol (20 ml) and transported using ultrasonic humidification and a N_2 carrier gas (4 $L.min^{-1}$) into a heated reactor (500 °C) where the FTO electrode was housed. When the reaction was complete (~ 1 hour), the reactor was allowed to cool to room temperature. The as-deposited coatings were brightly yellow in color and strongly adhered to the FTO substrate.

Physical characterization: X-ray diffraction (XRD) patterns were measured with a modified Bruker-Axs D8 diffractometer with parallel beam optics equipped with a PSD LinxEye silicon strip detector. The instrument uses a Cu source for X-ray generation (V = 40 kV, I = 30 mA) with Cu $K_{\alpha1}$ (λ = 1.54056 Å) and Cu $K_{\alpha2}$ radiation (λ = 1.54439 Å) emitted with an intensity ratio of 2:1. The incident beam was kept at 1° and the angular range of the patterns collected between $10 \leq 2\Theta° \leq 66$ with a step size of 0.05 ° and time step 60 s/°. X-ray photoelectron spectroscopy (XPS) was carried out using a Thermo K-Alpha spectrometer with monochromated Al K_α radiation at different positions across the substrate. Survey scans were

collected over the 0 – 1400 eV binding energy range with 1 eV resolution and a pass energy of 200 eV. More focused scans were collected at the specific binding energy regions of C 1s, Cl 2p, F 1s, Mg 1s, O 1s, Sn 3d and V 3p with 0.1 eV resolution. An Ar-ion gun was used to etch the surface layers of samples to record a depth profile for a sputtering time of 15 s per level (7 levels in total). Peaks were modelled using CasaXPS. Peak positions were calibrated to adventitious graphite (284.5 eV) and peak areas were adjusted using the appropriate sensitivity factors to determine the population fraction of each state. The surface morphology was investigated using scanning electron microscopy (SEM) on a JEOL-6400 SEM field emission instrument.

Electrochemical Performance: The electrochemical performance of the samples was studied using a three-electrode cell as reported previously [15,16], in 0.075 M, aqueous $MgCl_2$ solution and a scan rate of 10 mV s^{-1} for a potential ranging -1.5 V - +1.0 V. Furthermore, cyclic voltammograms were obtained for scan rates 20 mV s^{-1}, 40 mV s^{-1}, 60 mV s^{-1}, 80 mV s^{-1} and 100 mV s^{-1}. Chronopotentiometric measurements were performed at specific currents of 2.4 A g^{-1}, 3.9 A g^{-1}, 4.2 A g^{-1}, 4.5 A g^{-1}, 5 A g^{-1} and 5.9 A g^{-1} for a potential range of -1.0 V - -0.5 V. Electrochemical impedance spectroscopy (EIS) curves were obtained for alternating current (AC) amplitude of 5.0 mV and set potential of -1.0 V over the frequency range of 10 mHz-100 kHz.

3. Results and Discussion

XRD of the pristine V_2O_5 material (Figure 1A) presents four characteristic peaks (●) at 15.2 ^{o}, 20.0 ^{o}, 21.6 ^{o} and 31.0 ^{o} with respective Miller indices (200), (001), (101) and (400), which are consistent with the formation of orthorhombic V_2O_5 [17]. The other indicated peaks (■) are due to the FTO electrode underneath [18]. For the magnesiated sample, there is only one peak observed due to orthorhombic V_2O_5 at 30.5 ^{o}, which is slightly shifted by 0.5 ^{o} compared with the pristine. Similar behavior is supported by others [13,19]. The effect of Mg^{2+}

intercalation on the structure of V_2O_5 was studied by SEM showing agglomerations of grains. These grains are less uniformly distributed across the substrate in pristine V_2O_5 (Figure 1B) as compared with magnesiated V_2O_5 (Figure 1C), which indicates the formation of more compact triangular grains upon Mg-ion intercalation.

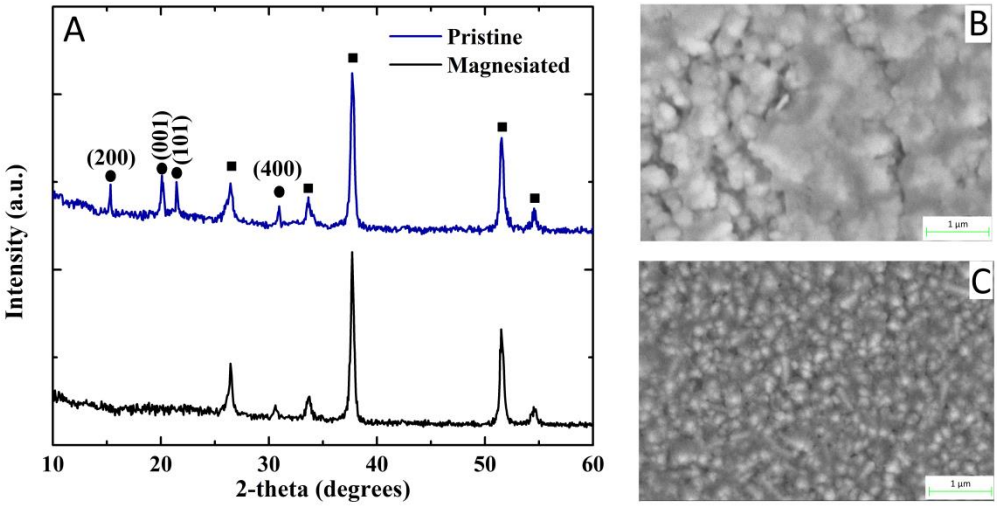

Figure 1. A: XRD (circles represent reflections from orthorhombic V_2O_5 and squares represent reflections from the fluorine-doped tin oxide substrate), **B & C:** SEM images at x100,000 magnification of pristine and magnesiated V_2O_5 cathodes respectively.

XPS are shown in Figure 2A. In the pristine V_2O_5 cathode, the V $2p_{3/2}$, V $2p_{1/2}$ and O 1s environments are centered at binding energies of 517.5 eV, 524.9 eV and 530.3 eV respectively, and correspond to the presence of V^{5+} and O^{2-} in a V_2O_5 environment [20,21]. There is also an additional peak at 532.5 eV due to the presence of chemisorbed OH groups on the surface of the cathode [14]. In the case of the magnesiated sample, the Mg 1s peak was observed at approximately 1304 eV indicating the presence of intercalated Mg^{2+} in the V_2O_5 electrode [22], while the peak due to chemisorbed OH groups at 532.5 eV disappears. This is attributed to the ease in which water enters and exits the structure upon cycling due to a weak interaction with the metal oxide framework [23]. XPS measurements were conducted at several positions across the substrate. In both the pristine and magnesiated V_2O_5 samples, the presence of V_2O_5 was consistently observed, which was indicative of a homogeneous coating.

Compositional depth profile measurements showed that Mg-ions were intercalated within the host V_2O_5 structure, and not merely at the surface (Figure 2B). It is worth mentioning that no chlorine atoms were detected in the elemental composition of the magnesiated sample, which confirmed that the Mg-ions present in the V_2O_5 cathode was not due to residual $MgCl_2$ salt from the electrolyte.

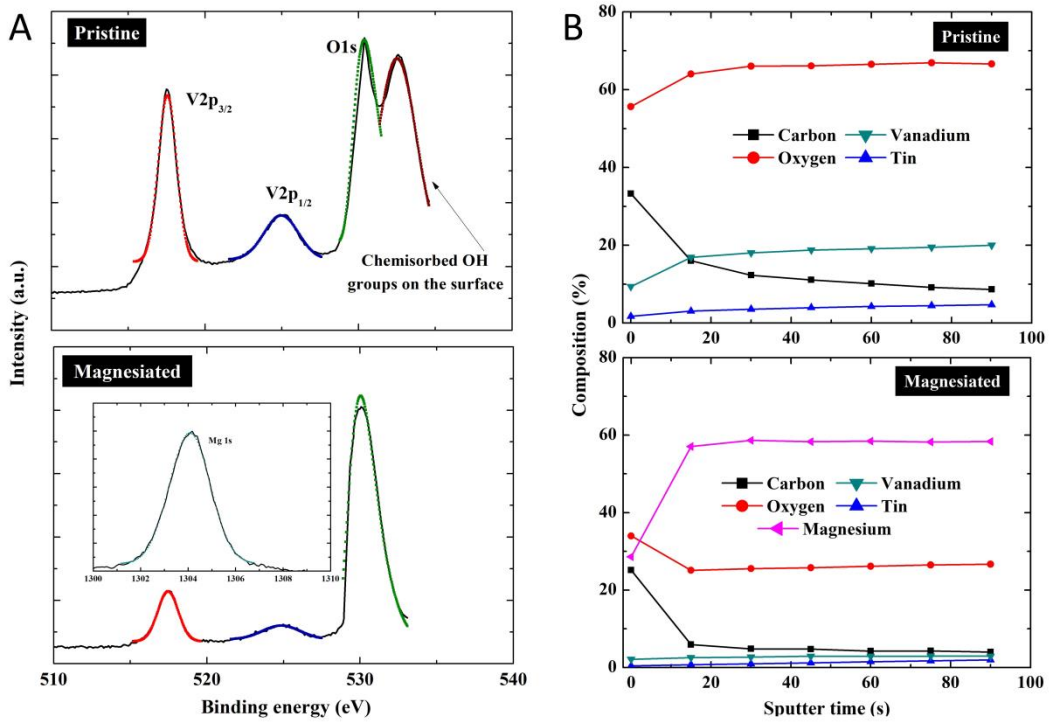

Figure 2. A: Surface XPS measurements (V 2p and O 1s binding energy region) of pristine and magnesiated V_2O_5 cathodes (inset shows Mg 1s binding energy region in the magnesiated sample), **B:** XPS depth profile composition measurements of pristine and magnesiated V_2O_5 cathodes.

Figure 3A presents the cyclic voltammograms up to 2000 scans for the V_2O_5 cathode in $MgCl_2$, 0.075 M. The potential was reversibly swept from -1.5 V to +1.0 V (versus Ag/AgCl) at a scan rate of 10 mV s^{-1}. The cyclic voltammograms exhibit an oxidation peak at -0.70 V and a reduction peak at -1.07 V corresponding to the respective de-intercalation ($Mg \rightarrow Mg^{2+} + 2e^-$) and intercalation ($Mg^{2+} + 2e^- \rightarrow Mg$) of Mg^{2+} into the V_2O_5 cathode. The reversible nature of the redox peaks shows that AACVD coating of V_2O_5 are active cathode materials for MIBs. The intensity of the peaks increase as the scan number increases to 500, indicating

the capacity to store Mg^{2+} increases with cycling [24]. This is attributed to the interfacial reactions that inevitably occur in the cathode material. However, when the electrode is cycled for more than 1000 scans, peak intensities remain unchanged, indicating the high stability of these V_2O_5 cathodes. The effect of the scan rate ranging from 10, 20, 40, 60, 80 and 100 mV s^{-1} on V_2O_5 is shown in Figure 3B. As the scan rate was increased the current density also increased, yet the shape of the curves remain unchanged, which overall indicates a high rate capability [25].

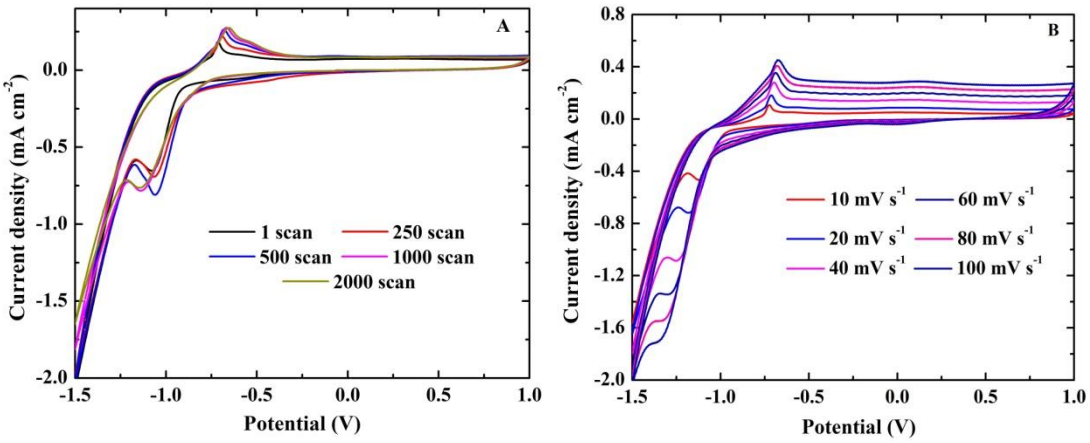

Figure 3. A: Cyclic voltammograms of V_2O_5 cathodes after 1, 250, 500, 1000, 2000 scans measured in 0.075 M $MgCl_{2\,(aq)}$ (scan rate = 10 mV s^{-1}). **B**: Cyclic voltammograms for the 1st scan using scan rates of 10, 20, 40, 60, 80 and 100 mV s^{-1}.

The discharge curves of the AACVD grown V_2O_5 cathodes are shown in Figure 4A under specific currents of 2.4, 3.9, 5.9 A g^{-1} and applied potentials ranging from -1.0 V to -0.5 V. A peak at approximately -0.95 V is observed suggesting the one-step discharging process (de-intercalation) for all specific currents applied. The specific discharge capacity was 427 mAh g^{-1} at the highest specific current applied with capacity retention of 82 % after 2000 scans retaining the staircase shape (Figure 4B). After 1000 continuous charge-discharge scans, the agglomerations appear thicker and larger most likely due to volume changes associated with Mg^{2+} intercalation (Figure 4A inset). The presence of V_2O_5 after 1000 scans is also supported by XPS, but with lower intensity compared with the pristine (Figure 4C). Rate capability is also an important parameter for batteries and is evaluated at specific currents of 2.4 up to 5.9

A g^{-1}, as shown in Figure 4D. The material presents higher specific discharge capacity at 5.9 A g^{-1} (427 mAh g^{-1}) than at 2.4 A g^{-1} (170 mAh g^{-1}). Additionally, the cathode could still deliver a specific discharge capacity of 425 mAh g^{-1}, when the specific current was returned to 5.9 A g^{-1}, corresponding to capacity retention of 99 % of the original value, which suggests good structural stability and high reversibility. The upward trend of the specific discharge capacity with increasing specific current can be due to the fast diffusion kinetics of Mg^{2+} in the metal oxide framework. This is also suported by cyclic voltammetry measured at increasing scan rates (Figure 3B). Overall, as the specific current is increased, this shows that the diffusion depth of Mg^{2+} is sufficent to intercalate within the bulk of the V_2O_5 nanostructure. It is interesting to note that there is little fading of the capacity for any of the specific currents applied (Figure 4E). These phenomena may be attributed to the well-defined nanostructures (Figure 1B & C), and their advantageous shape and distribution for Mg^{2+} intercalation.

Using an analogous aqueous $MgCl_2$ electrolyte, Zhang *et al.* investigated cathodes for MIBs composed of $Mg_{1.1}Mn_6O_{12}.4.5H_2O$. Their materials initially showed specific discharge capacities of ~100 mAh g^{-1} that decreased after 200 cycles to ~90 mAh g^{-1} [22]. Using non-aqueous electrolytes, Tepavcevic *et al.* studied nanostructured V_2O_5 bilayer cathodes for MIBs that showed specific discharge capacities of ~240 mAh g^{-1} [26]. Yu *et al.* investigated V_2O_5 powders in a propylene carbonate electrolyte that showed specific discharge capacities of ~160 mAh g^{-1} that decreased substantially to ~40 mAh g^{-1} in less than 10 cycles [27]. Imamura *et al.* investigated sol-gel V_2O_5/ carbon composite cathodes for MIBs in an acetonitrile electrolyte that showed high specific discharge capacities of ~540 mAh g^{-1} [28]. Gershinsky et al. studied monolithic V_2O_5 thin-film cathodes in non-aqueous solvents specific discharge capacities ranging between 150–180 mAh g^{-1} [29]. In this article, and using an aqueous electrolyte, our V_2O_5 cathodes showed high specific discharge capacities as high as 427 mAh g^{-1}, with little loss in performance after several hundred cycles (82% retention of

capacity after 2000 cycles under a high specific current of 5.9 A g^{-1}). It is also interesting to mention that in aqueous rechargeable Li-ion batteries, V_2O_5 exhibits poor capacity retention (15 % after 40 cycles) due to the dissolution of vanadium ions, accompanied by crystal structure changes and amorphization [30]. This can be inhibited using: a) polymeric compounds keeping the structural stability after 40 electrochemical cycles [24], b) a V_2O_5 xerogel that effectively improves capacity retention (89 % after 100 cycles) [31] and c) a hybrid composite (V_2O_5 nanowires and multi-walled carbon nanotubes) that retain the initial capacity of 110 mAh g^{-1} with negligible loss up-to 500 cycles [32].

Finally, the effect of continuous Mg^{2+} charging-discharging on the electron transport and recombination properties of the AACVD V_2O_5 cathodes is studied by EIS measurements as shown in Figure 4F. It can be observed that all Nyquist plots are composed of a partial semicircle in accordance with the charge transfer resistance (R_{ct}) at high frequencies and a linear part in accordance with the diffusion-controlled Warburg impedance at low frequencies. The intercept of the high frequency arc and x-axis is ascribed to the resistance of the electrolyte (R_s). The plots were further fitted using the equivalent circuit as indicated in Figure 4F inset consisting of the R_{ct}, R_s (solution resistance), a constant phase element and the Warburg impedance. The experimental data is represented by the symbols, while the data fitted by Z-view software by the solid lines. The R_{ct} considered as the rate-determining step during the charge-discharge process [33]. Therefore, the smaller the diameter of the semicircle is, the smaller the R_{ct} will be (higher specific capacitance). Both charge resistance (6 to 7.5 Ω for the 1^{st} to 1000^{th} scan) and ionic diffusion rate (the slope of the 500^{th} and the 1000^{th} scan coincide) endow the AACVD V_2O_5 cathodes with sustainable capacitive performance.

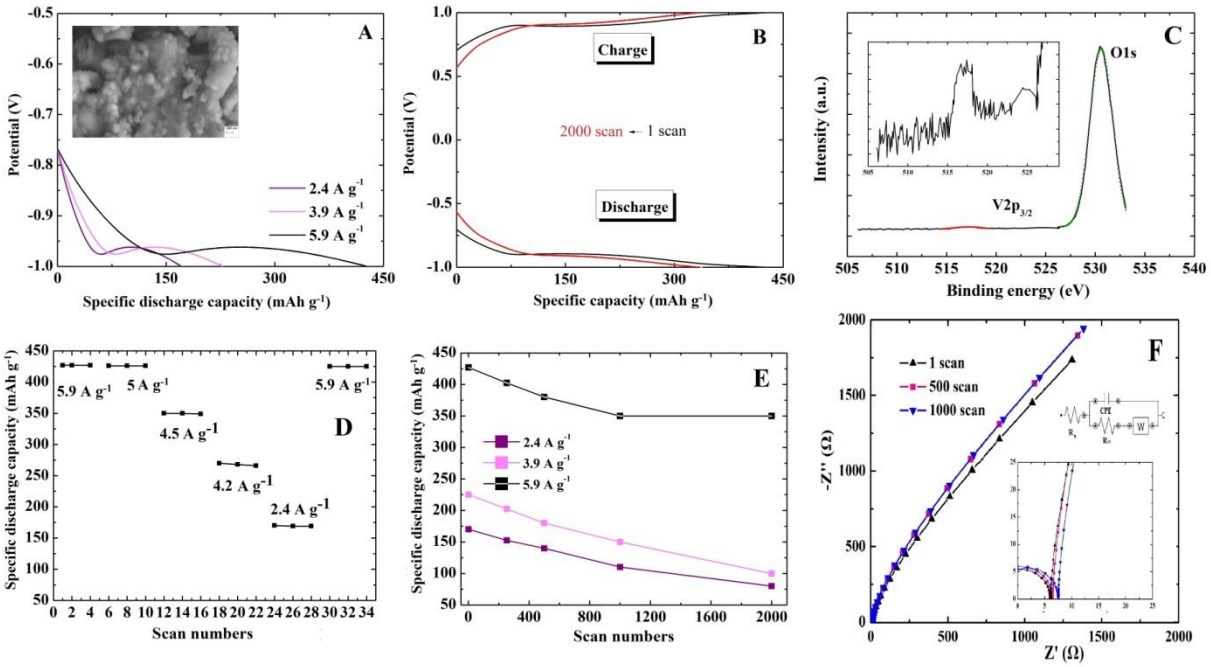

Figure 4. A: Chronopotentiometric curves for the V_2O_5 cathodes at a specific current of 2.4 A g^{-1}, 3.9 A g^{-1} and 5.9 A g^{-1} for potentials ranging from -1.0 V to -0.5 V. SEM of the sample after 1000 scans is shown in the inset. **B:** Chronopotentiometric curves for the V_2O_5 cathode under constant specific current of 5.9 A g^{-1} for potentials ranging from -1.0 V to +1.0 V for 1 and 2000 scans. **C:** XPS of the V_2O_5 cathode after 1000 continuous charge-discharge scans **D:** Rate capability of the sample at different specific current values ranging from 5.9 A g^{-1} to 2.4 A g^{-1} and then back to 5.9 A g^{-1}. **E:** Specific discharge capacity values as a function with scan number at 2.4 A g^{-1}, 3.9 A g^{-1} and 5.9 A g^{-1}. **F:** Nyquist plots of the measured (symbols) and fitted (solid lines) impedance spectra of the V_2O_5 cathode for the 1st, 500th and the 1000th scan. All measurements were performed in 0.075 M $MgCl_{2\,(aq)}$.

4. Conclusions

In summary, we have developed an aerosol-assisted chemical vapour deposition (AACVD) process for the upscalable growth of nanostructured V_2O_5 cathodes. These cathodes show promising performance for Mg-ion storage in terms of: (a) the high specific discharge capacity 427 mAh g^{-1}, with a capacity retention of 82 % after 2000 cycles measured at a high specific current of 5.9 A g^{-1}, and (b) the high rate capability, good structural stability and high reversibility. The promising performance observed herein opens up new opportunities for the upscalable production of Mg-ion batteries for the automotive and energy storage sectors.

References

[1] J. -Z. Guo, X. -L. Wu, F. Wan, J. Wang, X. -H. Zhang, R. -S. Wang, *Chem. Eur. J.* **2015**, *21*, 17371.

[2] J. -Z. Guo, P. -F. Wang, X. -L. Wu, X. -H. Zhang, Q. Yan, H. Chen, J. -P. Zhang, Y.-G. Guo, *Adv. Mater.* **2017**, *29*, 1701968.

[3] J. Su, X. –L. Wu, J. –S. Lee, J. Kim, Y.-G. Guo, *J. Mater. Chem. A* **2013**, *1*, 2508.

[4] P. Mei, X. –L. Wu, H. Xie, L. Sun, Y. Zeng, J. Zhang, L. Tai, X. Guo, L. Cong, S. Ma, C. Yao, R. Wang, *RSC Adv.* **2014**, *4*, 25494.

[5] M. Armand, J. –M. Tarascon, *Nature* **2008**, *451*, 652.

[6] J. B. Goodenough, K. –S. Park, *J. Am. Chem. Soc.* **2013**, *135*, 1167.

[7] D. Aurbach, Z. Lu, A. Schechter, Y. Gofer, H. Gizbar, R. Turgeman, Y. Cohen, M. Moshkovich, E. Levi, *Nature* **2000**, *407*, 724.

[8] Y. S. Guo, F. Zhang, J. Yang, F. F. Wang, Y. N. NuLi, S. Hirano, *Energy Environ. Sci.* **2012**, *5*, 9100.

[9] Y. L. Liang, R. J. Feng, S. Q. Yang, H. Ma, J. Liang, J. Chen, *Adv. Mater.* **2011**, *23*, 640.

[10] Y. Bai, L. Zhao, C. Wu, H. Li, Y. Li, F. Wu, *ACS Appl. Mater. Interfaces* **2016**, *8*, 2857.

[11] S. H. Ng, T. J. Patey, R. Buechel, F. Krumeich, J. Z. Wang, H. K. Liu, S. E. Pratsinis, P. Novak, *Phys. Chem. Chem. Phys.* **2009**, *11*, 3748.

[12] E. Armstrong, D. McNulty, H. Geaney, C. O'Dwyer, *ACS Appl. Mater. Interfaces.* **2015**, *7*, 27006.

[13] G. Gershinsky, H. Deong Yoo, Y. Gofer, D. Aurbach, *Langmuir* **2013**, *29*, 10964.

[14] S. Tepavcevic, Y. Liu, D. Zhou, B. Lai, J. Maser, X. Zuo, H. Chan, P. Král, C. S. Johnson, V. Stamenkovic, N. M. Markovic, T. Rajh, *ACS Nano* **2015**, *9*, 8194.

[15] D. Vernardou, I. Marathianou, N. Katsarakis, E. Koudoumas, I. I. Kazadojev, S. O' Brien, M. E. Pemble, I. M. Povey, *Electrochim. Acta* **2016**, *196*, 294.

[16] D. Vernardou, D. Louloudakis, E. Spanakis, N. Katsarakis, E. Koudoumas, *New J. Chem.* **2014**, *38*, 1959.

[17] H. Yu, X. Rui, H. Tan, J. Chen, X. Huang, C. Xu, W. Liu, D. Y. W. Yu, H. Hoon Hng, H. E. Hoster, Q. Yan, *Nanoscale* **2013**, *5*, 4937.

[18] M. Lv, D. Zheng, M. Ye, L. Sun, J. Xiao, W. Guo, C. Lin, *Nanoscale* **2012**, *4*, 5872.

[19] Y. Liu, J. Li, Q. Zhang, N. Zhou, E. Uchaker, G. Cao, *Electrochem. Commun.* **2011**, *13*, 1276.

[20] S. Beke, L. Korosi, S. Papp, A. Oszko, L. Nanai, *Appl. Surf. Sci.* **2009**, *255*, 9779.

[21] J. Swiatowska-Mrowiecka, V. Maurice, S. Zanna, L. Klein, P. Marcus, *Electrochim. Acta* **2007**, *52*, 5644.

[22] H. Zhang, K. Ye, X. Huang, X. Wang, K. Cheng, X. Xiao, G. Wang, D. Cao, *J. Power Sources* **2017**, *338*, 136.

[23] P. Novak, W. Scheifele, F. Joho, O. Haas, *J. Electrochem. Soc.* **1995**, *142*, 2544.

[24] D. He, D. Wu, J. Gao, X. Wu, X. Zeng, W. Ding, *J. Power Sources* **2015**, *294*, 643.

[25] L. Shen, S. Chen, J. Maier, Y. Yu, *Adv. Mater.* **2017**, 1701571.

[26] S. Tepavcevic *et al.*, *ACS Nano*. **2015**, 9, 8194–8205

[27] L. Yu, X. Zhang, *J. Colloid Interface Sci.* **2004**, 278, 160–165

[28] D. Imamura, M. Miyayama, M. Hibino, T. Kudo, *J. Electrochem. Soc.* **2003**, 150, A753

[29] G. Gershinsky, H. D. Yoo, Y. Gofer, D. Aurbach, *Langmuir*. **2013**, 29, 10964–10972

[30] H. Wang, Y. Zeng, K. Huang, S. Liu, L. Chen, *Electrochim. Acta* **2007**, *52*, 5102.

[31] I. Stojković, N. Cvjetić, I. Pašti, M. Mitrić, S. Mentus, *Electrochem. Commun.* **2009**, *11*, 1512.

[32] W. Tang, X. Cao, Y. Zhu, Y. Yue, Y. Shi, Y. Wu, K. Zhu, *J. Mater. Chem.* **2012**, *22*, 20143.

[33] G. G. Amatucci, F. Badway, A. Singhal, B. Beaudoin, G. Skandam, T. Bowmer, I. Plitz, N. Pereira, T. Chapman, R. Jaworski, *J. Electrochem. Soc.* **2001**, *148*, A940.